

ORIGINAL RESEARCH ARTICLE

Characterization of coatings on metallic nanoparticles by surface-enhanced Raman scattering (SERS) for environmental purposes

Sayed Amininejad¹  | Natalia P. Ivleva¹  | Thomas Baumann^{1,2} 

¹ Institute of Hydrochemistry, Technical Univ. of Munich, Marchioninstr. 17, Munich D-81377, Germany

² Chair of Hydrogeology, Technical Univ. of Munich, Arcisstrasse 21, Munich D-80333, Germany

Correspondence

Thomas Baumann, Chair of Hydrogeology, Technical University of Munich Arcisstr. 21, Munich, D-80333, Germany.
Email: tbaumann@tum.de

Assigned to Associate Editor Yan Jin.

Funding information

Deutsche Forschungsgemeinschaft (DFG), Grant/Award Number: 1536; Research Group 1536 INTERNANO, Project Ba 1592/6-2

Abstract

The increasing production and use of engineered inorganic nanoparticles (EINPs) escalate the risk for their unintended release into the environment. Coating of nanoparticles like natural organic matter (NOM) plays an important role in the stability, toxicity, and transport of nanoparticles. Surface-enhanced Raman scattering (SERS) has been proven to be a promising method to detect and characterize the coating on noble metal nanoparticles. Here, we report on the synthesis of core-shell Au–Ag nanoparticles (NPs) with a high SERS enhancement factor to study the exchange and competition of different coating agents with different binding abilities to simulate the release of NPs into a receiving environment with a number of potential coating agents. Suwannee River natural organic matter (SRNOM), 4-mercaptobenzoic acid (4-MBA), and 4-mercaptopyridine (4-MPy) were selected molecules for the experiments. The SERS experimental setup parameters such as aggregation size, laser excitation wavelength, and laser power were optimized before further experiments were conducted. It was shown that 4-MPy has a higher binding affinity than SRNOM and 4-MBA through the presence of simultaneous S and N atoms, which leads to dominating the coating process when two coating agents are present in the media at the same time. In addition, it was observed that 4-MPy and 4-MBA can replace the SRNOM coating on Au–Ag NPs.

Abbreviations: DLS, dynamic light scattering; EINP, engineered inorganic nanoparticle; EDX, energy-dispersive X-ray spectroscopy; EM, electromagnetic; 4-MBA, 4-mercaptobenzoic acid; 4-MPy, 4-mercaptopyridine; ICP–MS, inductively coupled plasma mass spectrometry; NOM, natural organic matter; NP, nanoparticle; SEM, scanning electron microscopy; SERS, surface-enhanced Raman scattering; SRNOM, Suwannee River natural organic matter; TEM, transmission electron microscopy; UV-vis, ultraviolet–visible.

This is an open access article under the terms of the [Creative Commons Attribution](https://creativecommons.org/licenses/by/4.0/) License, which permits use, distribution and reproduction in any medium, provided the original work is properly cited.

© 2020 The Authors. *Vadose Zone Journal* published by Wiley Periodicals LLC on behalf of Soil Science Society of America

1 | INTRODUCTION

The developments and innovations in nanotechnology and nanoscience have led to increasing use of engineered inorganic nanoparticles (EINPs) in numerous fields such as medicine, catalysis, photonics, electronics, agriculture, manufacturing technology, and energy due to their unique properties compared with their bulk material (Aragay, Pino, & Merkoci, 2012; Saha, Pal, Kundu, Basu, & Pal,

2009). The growing production and use of EINPs intensifies the risk for their discharge into the environment (Frimmel & Niessner, 2014; Sun, Gottschalk, Hungerbühler, & Nowack, 2014). Soil and water are two main environmental compartments where nanoparticles (NPs) might finally sink. The predicted release scenarios demonstrate that landfills (~63–91%) and soil (~8–28%) receive the largest portion of emitted NPs in the environment, followed by aquatic environment (~7%) (Bundschuh et al., 2018). Therefore, NPs impose a great risk for soil quality in the vadose zone, as well as potential risks for groundwater quality. To understand toxicity and fate of NPs in the environment, it is important to study the chemical nature of NPs, as well as their coatings (Wang, Zhang, Zhao, & Xing, 2016). Coating of NPs can alter their stability, mobility, and toxicity in the host media (Baalousha, Nur, Römer, Tejamaya, & Lead, 2013; El Badawy, Aly Hassan, Scheckel, Suidan, & Tolaymat, 2013; El Badawy et al., 2011; Gao et al., 2012). Adsorption of natural organic matter (NOM) is a controlling factor for stability of Au NPs with different capping agents (Stankus, Lohse, Hutchison, & Nason, 2011). The sorption of fulvic and humic acids, as well as Suwannee River humic acid, to Ag NPs was reported to increase the stability of NPs (Huynh & Chen, 2011; Li, Lenhart, & Walker, 2010). It has been observed that soil organic matter, on the one hand, accelerates aggregation of Ag NPs by bridging flocculation but, on the other hand, can stabilize them through electrostatic and steric effects (Klitzke, Metreveli, Peters, Schaumann, & Lang, 2015; Philippe & Schaumann, 2014). The presence of coatings can increase the mobility and decrease the retention of Ag NPs in soil. That can be attributed to the blocking of solid-phase sites that were initially available for retention of Ag NPs (He, Wang, & Zhou, 2019). Among the different methods implemented to characterize the coating of NPs, surface-enhanced Raman scattering (SERS) is an emerging technology that has shown great potential for detection of different coatings on noble metal NPs (Kühn, Ivleva, Klitzke, Niessner, & Baumann, 2015; Marsich et al., 2012). At least two principal mechanisms contribute to the enhancement: the electromagnetic (EM) enhancement and chemical enhancement (Kneipp, Kneipp, Itzkan, Dasari, & Feld, 2002; Schlücker, 2014). The EM enhancement occurs when the laser excites the surface plasmons and creates an EM field on the nanometer scale of SERS substrates. Chemical enhancement takes place when coating agent forms a chemical bond with metal surface and an electronic coupling is involved in between (Valley, Greeneltch, Van Duyne, & Schatz, 2013). The EM enhancement decreases strongly with growing distance (d^{-12}) from the surface of NP (Kneipp et al., 2002; Schlücker, 2014). It is believed that SERS can be effectively obtained from molecules located within 1–5 nm of

Core Ideas

- SERS was successfully used to characterize different coatings on noble metal NPs.
- Different parameters were investigated to optimize the reproducibility of SERS measurements.
- Competition of several coating agents with different binding affinities was studied.

the NP surface, although the exact distance is still up for debate (Kumari, Kandula, & Narayana, 2015; Shanthil, Thomas, Swathi, & George Thomas, 2012). The advantage of SERS is that the signal of conventional Raman techniques is increased by localized surface plasmon resonance (EM enhancement) and an increased Raman cross section (chemical enhancement) of substances in close vicinity of noble metal NPs. Surface-enhanced Raman scattering can characterize the functional groups of organic coatings that interact with the NPs including NOM and pesticides. In a study conducted by our group, SERS was implemented to characterize humic acid coating on Ag NPs under environmentally relevant conditions. Also, it was found that Ag NP treated with river water or soil suspension can be naturally coated with humic acid (Kühn et al., 2015). In another study, SERS has been successfully implemented to analyze thiram fungicide in soil suspension without any pretreatment with a detection limit of 0.148 mg kg⁻¹ (Lin et al., 2019). Another group of researchers have also applied SERS technique for determination of chlorpyrifos pesticide residues in soil (He, Xiao, Dong, & Nie, 2019). Despite the increasing number of SERS applications in different fields like environmental pollutants detection, food chemistry, and forensic science, reproducibility of measurements and consistent enhancement are the main limitations of this method (Cui, Li, Deng, Chen, & Wang, 2017; Guo et al., 2015; Kurouski & Van Duyne, 2015; Xu, Gao, Han, & Zhao, 2017; Zhao, Zhang, Li, Ji, & Liu, 2016). There are several parameters that need to be optimized in order to achieve SERS responses for characterization of NOM coatings on metallic NPs. Different factors like type of NP, size, morphology, and surface chemistry of NPs can alter the performance of SERS (Tian, Bonnier, Casey, Shanahan, & Byrne, 2014). In general, noble metal NPs within a size range of 10–200 nm show SERS activity, and NPs smaller than 10 nm or bigger than 200 nm exhibit very weak or no SERS enhancement. Noble metal NPs with a size range of 10–100 nm show an optimal SERS (Guo et al., 2015; Moskovits, 2005; Stamplecoskie, Scaiano, Tiwari, & Anis, 2011). In addition, the NPs used for the experiments

should be reproducible and easy to synthesize. Laser excitation wavelength has an effect on the experiment and should be selected in order to maximize scattering efficiencies and minimize the fluorescence background from the sample at the same time. Visible excitation lasers (e.g. 488, 514, 532, and 633 nm) are typically used for the measurements, but other excitation wavelengths from the ultraviolet (UV, 325 nm) as well as near infrared (785 or 830 nm), are also implemented for the measurements (Cui, Wu, Wang, Ren, & Tian, 2010; Kalachyova, Lyutakov, Kostejn, Clupek, & Svorcik, 2015; Ren et al., 2003; Wen, 2007). The pH can influence the adsorption process between coating agent and NPs by changing the surface charge. Temperature, time, aggregation, and coating agent are some of the other factors influencing the result of SERS measurements (Das et al., 2009; Qian & Nie, 2008). The objective of this study was to implement and optimize SERS for measurement of NOM coatings on metallic NPs. Furthermore, exchange and competition of different coating agents with different binding abilities was studied to simulate the release of NPs into a receiving media with a number of potential coating agents with different adsorption coefficients.

2 | MATERIALS AND METHODS

2.1 | Chemicals

Trisodium citrate and silver nitrate were obtained from Merck (Germany). The $\text{HAuCl}_4 \cdot \text{H}_2\text{O}$ and 4-mercapto benzoic acid (4-MBA) were purchased from Sigma-Aldrich (USA). The 4-mercaptopyridine (4-MPy) was purchased from Sigma-Aldrich (Japan). Suwannee River NOM (SRNOM) was purchased from the International Humic Substances Society (USA).

2.2 | Synthesis of Au–Ag NPs

Citrate-reduced Au–Ag core-shell NPs were synthesized following a similar procedure as Song, Mao, Zhou, and Hu (2016). Fifty milliliters of 0.01% (w/w) HAuCl_4 was mixed and reduced with 750 μl 1% (w/w) sodium citrate solution and heated at 100 °C for 20 min under magnetic stirring until the color of solution changed from colorless to wine red. The synthesized Au NPs were used as seed particles for preparation of Au–Ag core-shell NPs. Two hundred and ninety microliters of 0.5% (w/w) AgNO_3 was added to the 50-ml boiling Au NP suspension. Finally, 0.5 ml of 1% (w/w) sodium citrate solution was slowly added to the stirring suspension and heated at 100 °C for 1 h. Then, heating was stopped and the suspension was cooled down to room

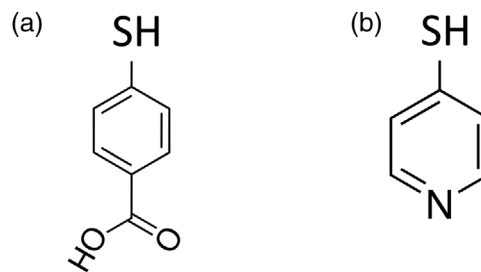


FIGURE 1 Chemical structure of (a) 4-mercaptobenzoic acid (4-MBA) and (b) 4-mercaptopyridine (4-MPy)

temperature for 2 h. The color of the final suspension was red–orange.

2.3 | Characterization of Au–Ag NPs

Ultraviolet–visible (UV-vis) spectroscopy, scanning electron microscopy (SEM) coupled with energy-dispersive X-ray spectroscopy (EDX), as well as transmission electron microscopy (TEM) were applied to confirm the successful synthesis of the core-shell NPs. Dynamic light scattering (DLS) was implemented to measure the hydrodynamic size of the NPs (Delsa Nano C, Beckman Coulter). The size and morphology of the NPs was characterized by using a Sigma VP 300 SEM (Carl Zeiss). The EDX measurements were conducted to understand the composition of the synthesized NPs using a XFlash 6 | 60 (BRUKER). Nanoparticles were additionally characterized by TEM using a JEM-1400plus with an acceleration voltage of 120 kV. Inductively coupled plasma mass spectrometry (ICP–MS) measurements were conducted at the Institute for Environmental Sciences at the University of Koblenz-Landau to evaluate the concentration of Au and Ag (XSeries 2, Thermo Scientific). For UV-vis measurements, NP suspensions were measured in semi-micro PMMA-cuvette using a SPECORD 250 PLUS (Analytic Jena). Deionized water was used as reference spectrum for UV-vis measurements.

2.4 | Preparation of coated Au–Ag NPs

Suwannee River NOM, 4-MBA, and 4-MPy were selected as sample molecules for the experiments. The chemical structures of 4-MBA and 4-MPy are shown in Figure 1. For optimization of SERS measurements for separate 4-MBA, 4-MPy, and SRNOM coatings, the Au–Ag NP suspension was added to coating solutions in equal parts with a final concentration of 10^{-5} mol L^{-1} and equilibrated for 2 h on an overhead shaker. Suwannee River NOM had a final concentration of 20 mg L^{-1} . Afterwards, samples were washed

two times via centrifugation for 15 min and resuspended in deionized water after removal of supernatant. The samples were also treated in an ultrasonic bath for 10 min to avoid formation of aggregates. The samples were kept in water bath filled with ice in order to avoid thermal damage to NOM. Finally, 10 μl of the suspension was placed on a silicon wafer to dry for SERS measurements.

To simulate competition of coating agents, two of the mentioned coating agents at concentrations of 10^{-5} mol L^{-1} for 4-MBA or 4-MPy and 20 mg L^{-1} for SRNOM, respectively, were mixed together and the Au–Ag NP suspension was added in equal parts to them. After shaking for 2 h on overhead shaker the samples were washed for two times as described above.

To simulate replacement of coating agents, the NPs were coated with SRNOM for 24 h on overhead shaker to ensure the coating. Consequently, 4-MBA or 4-MPy with a final concentration of 10^{-5} mol L^{-1} was added and the suspensions were shaking for 2 h before washing steps.

2.5 | SERS measurements of coated Au–Ag NPs

The SERS spectra were recorded by a LabRAM HR Raman microscope (Horiba, Jobin Yvon) using a He–Ne laser (633 nm) with 3.4 mW laser power at the sample. A 50 \times objective (numerical aperture = 0.75) was used with acquisition times of 2, 5, or 10 s. Replicate of each sample were made for three times, and spectra were obtained at least at five different points of each sample to verify the reproducibility of the spectra. Baseline correction was performed to obtain the final spectrum.

3 | RESULTS AND DISCUSSIONS

3.1 | Characterization of coated of Au–Ag NPs

The SEM and TEM images of the citrate-reduced Au–Ag NPs show uniform spheres with an approximate size of 35 nm (Figure 2). The results are in agreement with DLS measurements which reveal an approximate diameter of 33 nm.

The results of the EDX analyses show the presence of Au and Ag in elemental composition of the synthesized NPs. The spectrum contains characteristic peaks, which are assigned to Au and Ag (Figure 3).

The UV-vis spectrum of gold NPs shows a peak at 520 nm, which is in the adsorption peak region for gold. The peak of UV-vis spectrum for Au–Ag core-shell NPs shows a blue shift compared with the absorption peak of

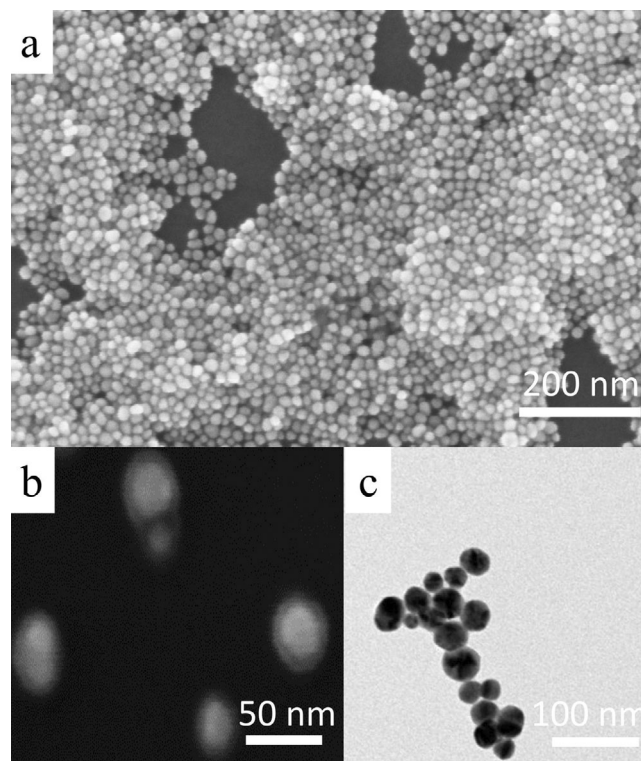


FIGURE 2 Scanning electron microscope (SEM) image of prepared Au–Ag nanoparticles, and transmission electron microscope (TEM) image of Au–Ag nanoparticles

Au NPs, which indicates the effective coating of Au NP seeds with Ag. Both UV-vis spectra show narrow peaks, which is indicative of relative monodisperse suspension (Figure 4). The Au–Ag NPs have a zeta potential value of -41 mV, which is less than -30 mV, and therefore the NPs are considered to be stable. The results prove the successful synthesis of core-shell NPs.

3.2 | Optimization of experimental parameters

To achieve reproducible SERS results as the main challenge for SERS analysis, the experimental parameters should be optimized at first. The optimum SERS conditions for different coating agents can be highly variable and, therefore, an optimum setup that fits for all of the coating agents should be implemented (Yaffe, Ingram, Graham, & Blanch, 2009).

Figure 5 shows the SERS spectra of selected coating agents on Au–Ag NPs after optimization of experimental parameters. The SERS spectra of 4-MPy is dominated by characteristic peaks at about 711, 1,006, 1,063, 1,097, 1,223, 1,580, and 1,609 cm^{-1} . The band at 1,091 cm^{-1} is representative of covalent binding of S to the Au–Ag as the result

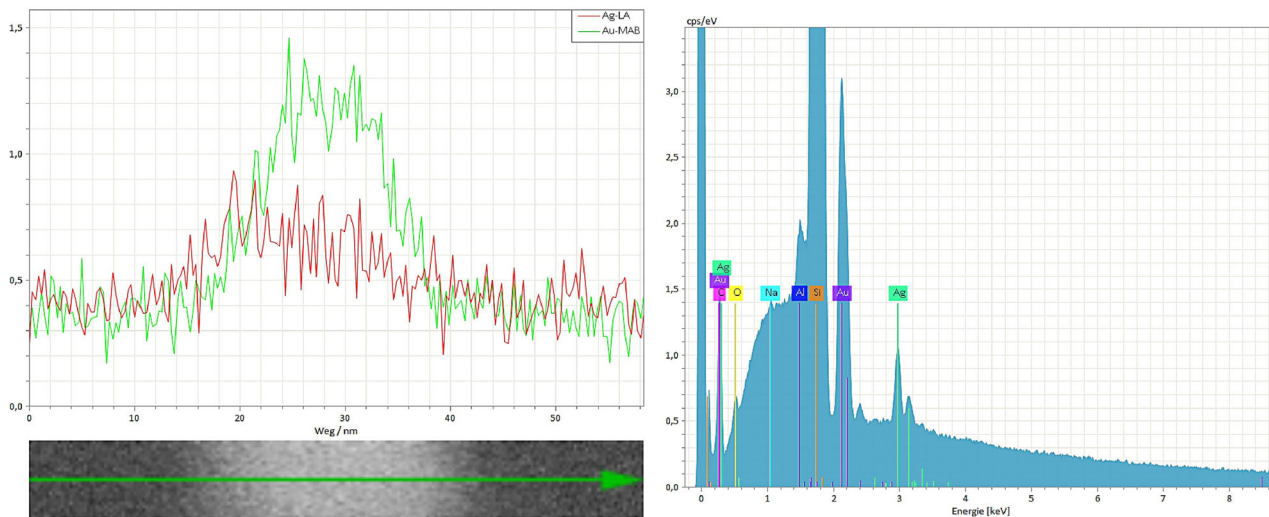


FIGURE 3 Energy dispersive X-ray analysis (EDX) of as-prepared Au-Ag nanoparticles

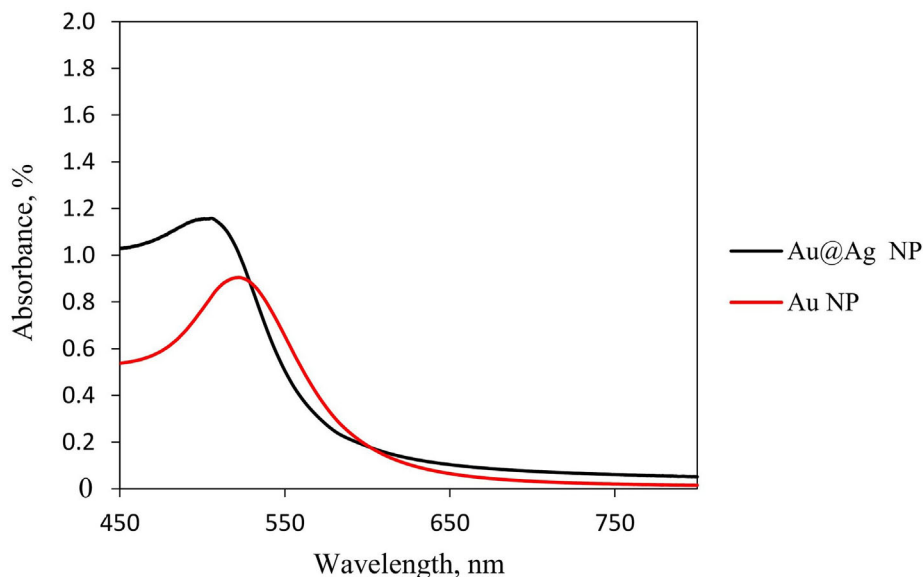


FIGURE 4 Ultraviolet-visible (UV-vis) spectra of Au-Ag and Au nanoparticles (NPs)

of the altered C-S bond on the ring vibrations. The peak around 711 cm^{-1} is indicative of the in-plane ring deformation with C-S. The bands at $1,580$ and $1,609\text{ cm}^{-1}$ are indicative of the ring stretch with N vibrations, and the bands at $1,063$ and $1,223\text{ cm}^{-1}$ are assigned to in-plane C-H vibrations. Furthermore, the band at around $1,006\text{ cm}^{-1}$ is assigned to the ring-breathing vibrations (Wang & Rothberg, 2005; Zhang, Bai, Shang, Zhang, & Mo, 2007). The two Raman peaks at $1,580$ and $1,609\text{ cm}^{-1}$ have been also attributed to N-deprotonation and N-protonation and are therefore being used as markers for the SERS-based pH sensors.

The SERS spectra of 4-MBA are dominated by two signals, one at about $1,585\text{ cm}^{-1}$ that arises from ν_{8a} aromatic-ring vibrations, and a band at about $1,076\text{ cm}^{-1}$ that is assigned to ν_{12} aromatic-ring vibrations processing C-S stretching characteristics (Ho & Lee, 2015). The band seen at about $1,424\text{ cm}^{-1}$ is attributed to symmetric stretching vibration of the carboxylate group, $\nu_s(\text{COO}^-)$.

The SERS spectra of SRNOM are dominated by two features at about $1,355$ and $1,575\text{ cm}^{-1}$, which are referred to as G peak (graphite peak) and D peak (disordered peak) in carbon analysis. The G peak is assigned to in-plane

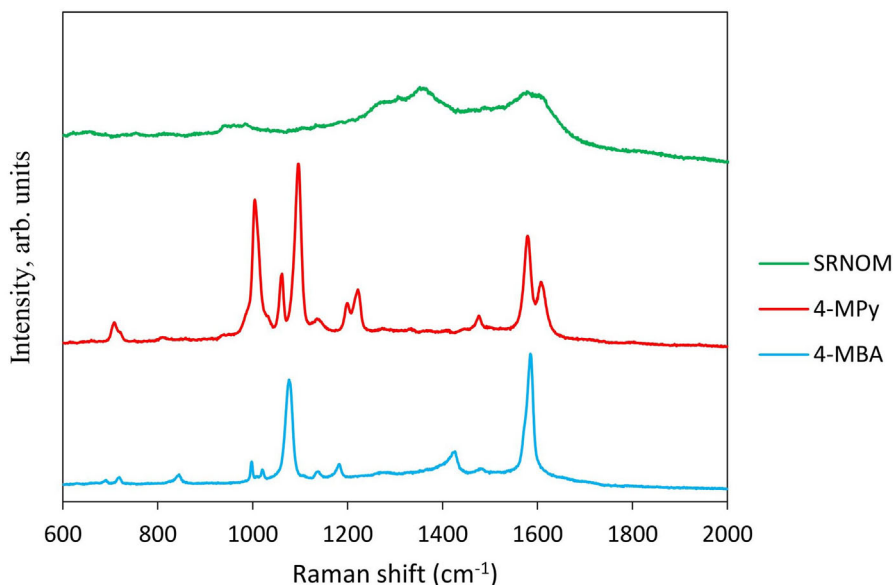


FIGURE 5 Surface-enhanced Raman scattering (SERS) spectra of selected coating agents on Au–Ag. SRNOM, Suwannee River natural organic matter; 4-MPy, 4-mercaptopyridine; 4-MBA, 4-mercaptobenzoic acid

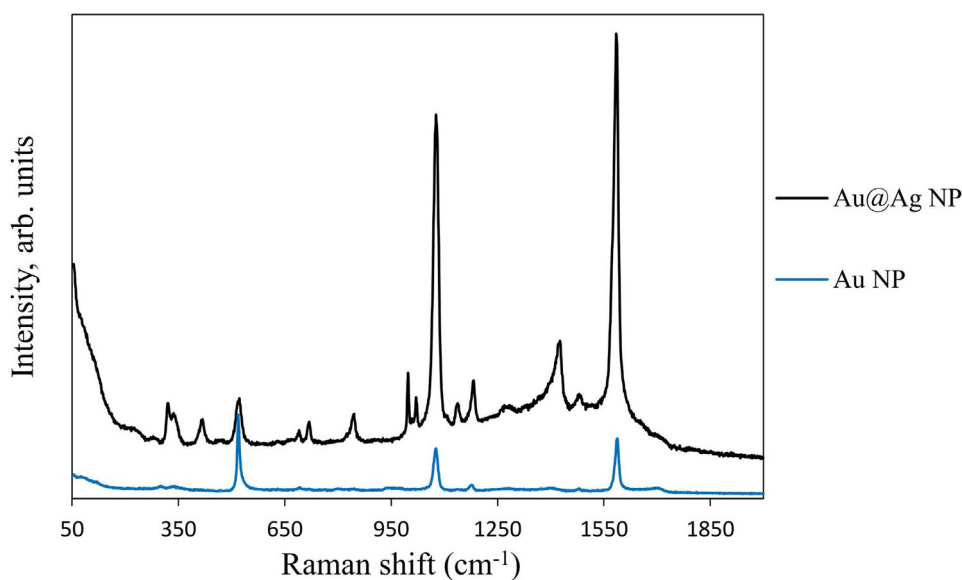


FIGURE 6 The surface-enhanced Raman scattering (SERS) spectra of 4-mercaptobenzoic acid (4-MBA) coated on the surface of Au nanoparticles (NPs) and Au–Ag NPs

bond-stretching motion of pairs of sp^2 atoms. The D peak is assigned to the breathing mode of sixfold aromatic rings (E_{2g} symmetry).

To confirm the effect of different NPs on SERS enhancement, we have compared the different SERS signals of Au NPs as the core with final Au–Ag NPs. Figure 6 shows that Au–Ag NPs exhibit a higher SERS enhancement factor than Au NPs. The spectra have been collected at the same measurement conditions. It has been reported that Ag NPs generate stronger SERS intensities than Au NPs

of the same size (Yuan, Fales, Khoury, Liu, & Vo-Dinh, 2013). However, synthesizing of monodisperse Ag NPs is still challenging. From the other side, Au NPs are more uniform (Dreaden, Alkilany, Huang, Murphy, & El-Sayed, 2012; Rycenga et al., 2011). Hence, Au–Ag NPs are an effective solution to synthesize more monodisperse NPs with high SERS enhancement.

The selection of proper laser wavelength is highly dependent on the application. To select the appropriate excitation wavelength, three different excitation

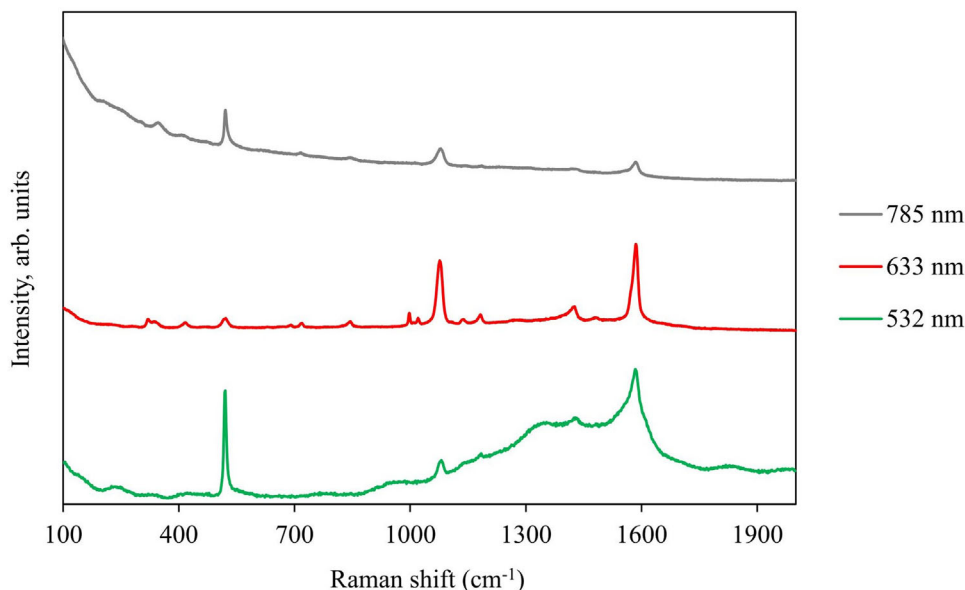


FIGURE 7 The surface-enhanced Raman scattering (SERS) spectra of 4-mercaptobenzoic acid (4-MBA) on the surface of Au-Ag nanoparticles (NPs) with different excitation wavelengths

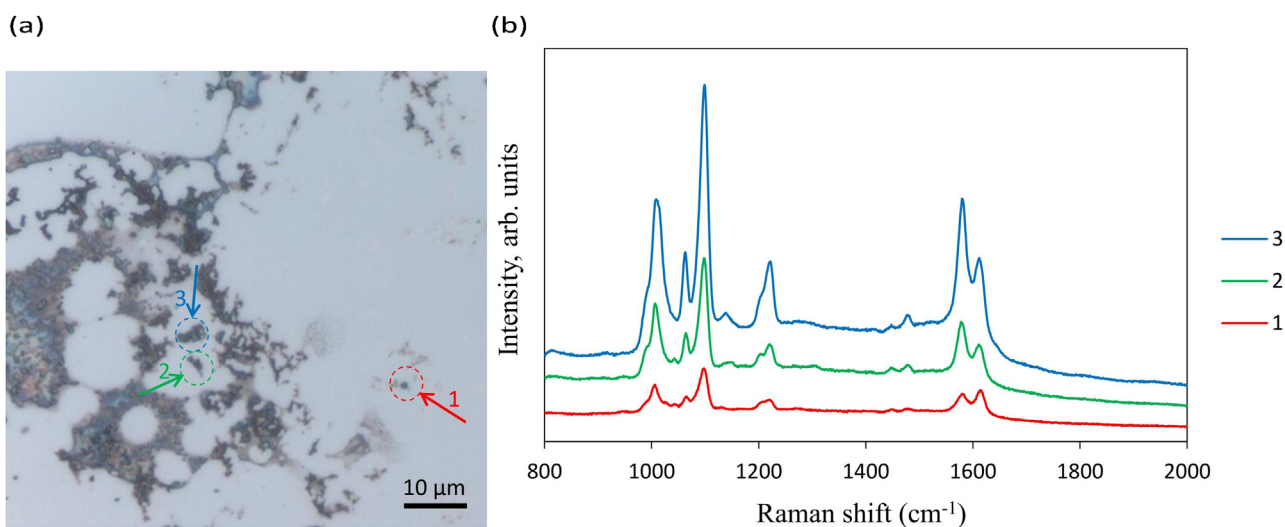


FIGURE 8 Effect of aggregation size on the surface-enhanced Raman scattering (SERS) spectra of 4-mercaptopyridine (4-MPy) on the surface of Au-Ag nanoparticles (NPs). (a) Selected aggregates with different sizes. (b) 4-MPy SERS spectra of selected aggregates

wavelengths of 532, 633, and 785 nm were tested. Figure 7 shows the recorded spectra of 4-MBA coated Au-Ag NPs with these laser excitation wavelengths. The use of a 532-nm excitation laser can lead to thermal decomposition of the NOM and the formation of amorphous C. The 633-nm laser provides a balance of high sensitivity and low fluorescence that is optimal for the experiments. The spectra obtained with a 785-nm laser show lower SERS enhancement. Therefore, further experiments were conducted using a 633-nm laser.

Figure 8 shows the effect of size of NPs aggregates on the SERS spectra of the 4-MPy coated Au-Ag NPs. With increasing the size of aggregate from less than 1 μm to almost 4 μm , more intensive SERS spectra are observed that can be attributed to formation of more hot spots. The formation of hot spots via aggregation is dependent on many factors such as size, shape, and also surface chemistry of the NPs (Schlücker, 2014). In colloidal suspensions, the formation of hot spots are stimulated by addition of aggregating salts like NaCl or KNO_3 , but this process is not

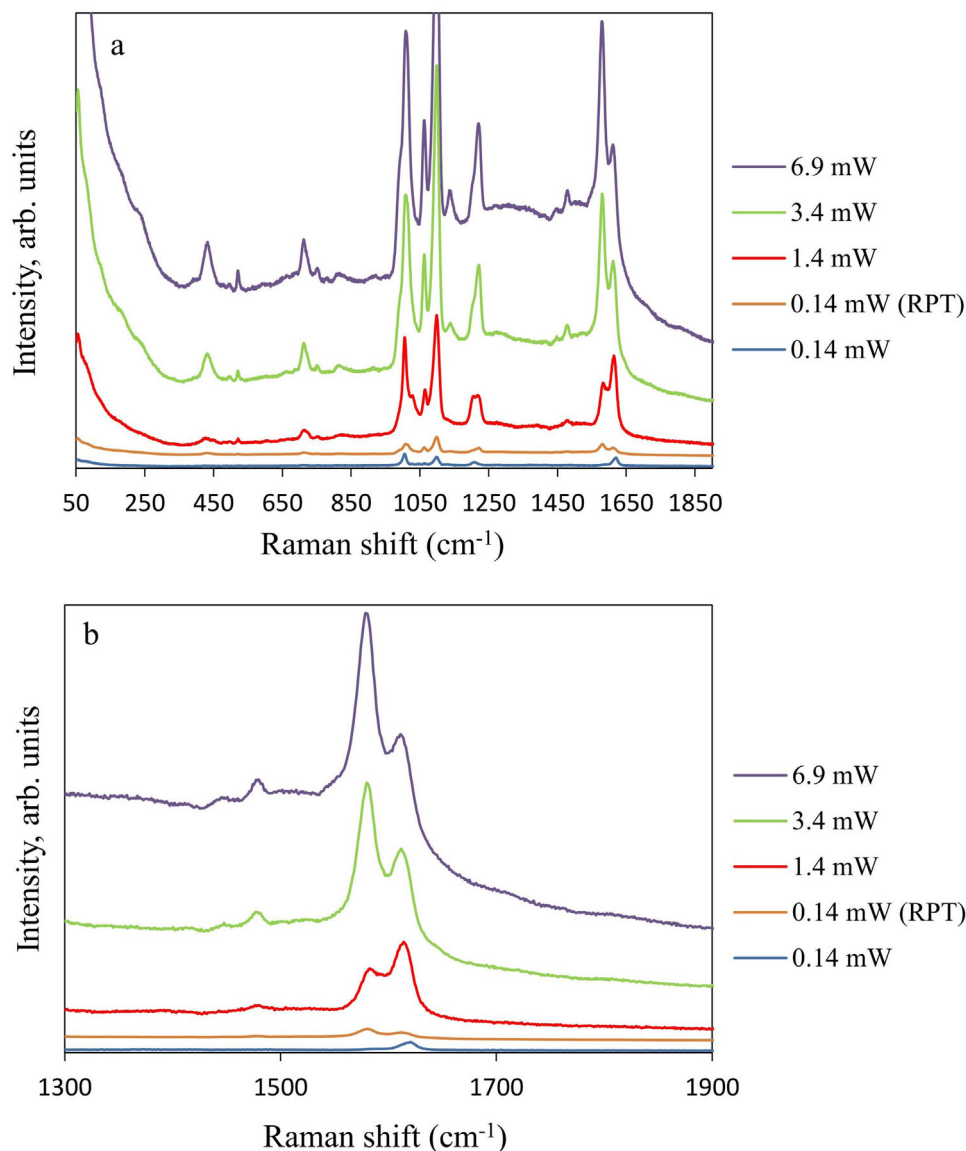


FIGURE 9 (a) Laser power dependency of mercaptopyrindine (4-MPy) surface-enhanced Raman scattering (SERS) spectra on the surface of Au-Ag nanoparticles (NPs) at the same location and (b) laser power-induced alteration of 4-MPy coating based on the intensity ratio of the two peaks appearing at 1,575 and 1,610 cm^{-1} (I_{1575}/I_{1610}) (RPT = second run)

well reproducible (Wei, Abtahi, & Vikesland, 2015; Yaffe et al., 2009).

Figure 9 shows spectra acquisition of 4-MPy coated Au-Ag NPs deposited on a silicon wafer, taken with different laser powers. It can be observed that increasing the laser power during measurements can also increase the intensity of SERS signal, but it also causes change of the structure of carbonaceous coating. Higher laser powers induce thermal damage to the structure of the coating suggested by appearance of the G and D peaks. In addition, the intensity ratio of peaks at 1,575 (I_{1575}) and 1,610 cm^{-1} (I_{1610}) is also changing by increasing the laser power.

Figures 9b and 10 illustrate the evolution of the ratio of I_{1575}/I_{1610} at different laser powers of 0.14, 1.4, 3.4, and 6.9 mW. It can be observed that the intensity ratio increases

with increasing the laser power. Finally, by changing the laser power from 6.9 mW back to 0.14 mW, the intensity ratio will stay constant and does not change. This phenomenon can show a laser power-dependent (thermal-dependent) change of the structure of 4-MPy coating on Au-Ag NPs leading to observed spectral changes. These changes can be attributed to double-end-bonded state (Au-Ag/4-MPy/Au-Ag) formation of coating via both sulfhydryl and pyridyl in the structure of 4-MPy (Zheng et al., 2014).

3.3 | Competition of coating agents

Figure 11 shows the competition of coating agents when two of them are available at the same time in the media and have contact with NPs. The spectra are collected

FIGURE 10 Laser power-induced alteration of mercaptopyrindine (4-MPy) coating based on the intensity ratio of the two peaks appearing at 1,575 and 1,610 cm^{-1} (I_{1575}/I_{1610}) (five replicates for each measurement point)

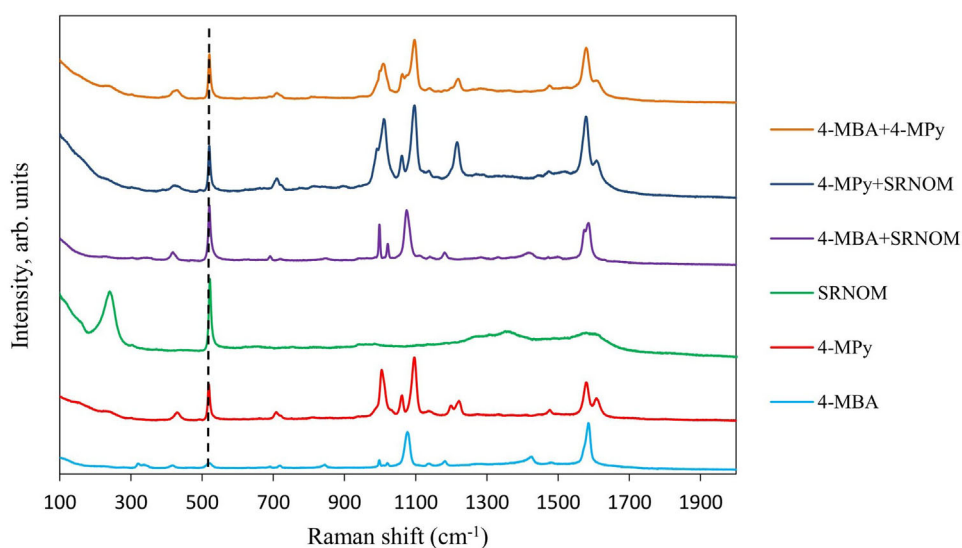
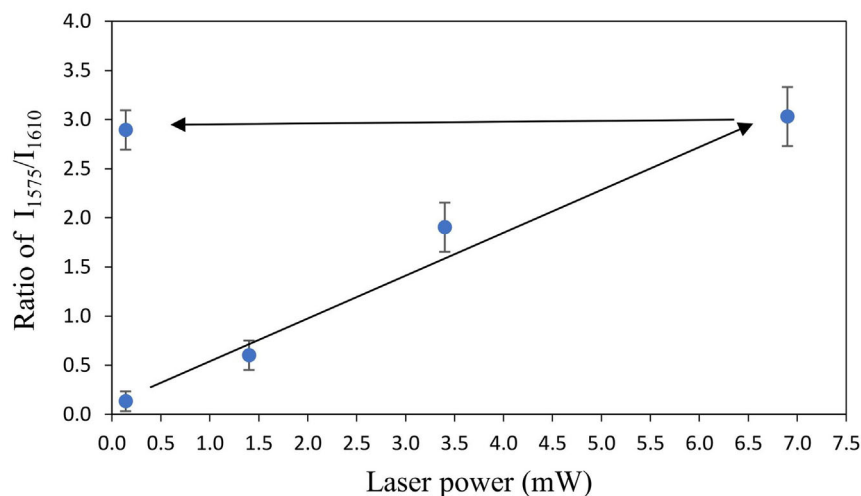


FIGURE 11 Comparison of binding of different coating agents and competition of coating agents at the same time under same optimized setup. 4-MBA, 4-mercaptopbenzoic acid; 4-MPy, 4-mercaptopyrindine; SRNOM, Suwannee River natural organic matter

at the same measurement conditions after optimization of the parameters. Figure 11 exhibits the characteristic signals of 4-MBA when 4-MBA and SRNOM were both present in the media, which shows that 4-MBA binds more strongly than SRNOM to the NPs. The more intense signals of 4-MBA and 4-MPy can be also explained by a higher cross section of these compounds. The same situation was observed when 4-MPy and SRNOM were both present in the NP-containing system and the spectrum showed the characteristics of 4-MPy, suggesting that 4-MPy also binds more strongly than SRNOM to the NPs. The competition between 4-MBA and 4-MPy showed that 4-MPy outcompeted 4-MBA and has binds more strongly with Ag–Au NPs. The results indicate that 4-MPy binds more strongly than the other two coating agents to the NPs. This may be explained by the pres-

ence of S and N atoms at the same time in 4-MPy, which leads to a stronger bond than just the S atom in 4-MBA.

Figure 12 exhibits the SERS spectrum of NPs coated with SRNOM after 24 h, and also the NP-containing systems exposed to a second coating agent for 2 h after 24 h of coating with SRNOM. The spectra indicate the characteristic signals of both coating agents at the same time. It shows that 4-MBA and 4-MPy bind to the NPs despite the SRNOM coating being previously formed. The band at 230 cm^{-1} represents the Ag–N vibration of the NPs (Dai, Zhang, Du, Huang, & Dang, 2005). Both 4-MPy and 4-MBA are smaller molecules than SRNOM molecules, and due to presence of a S atom in their molecular structure, they can strongly bind to the surface of the core-shell NPs, even when a coating has already formed.

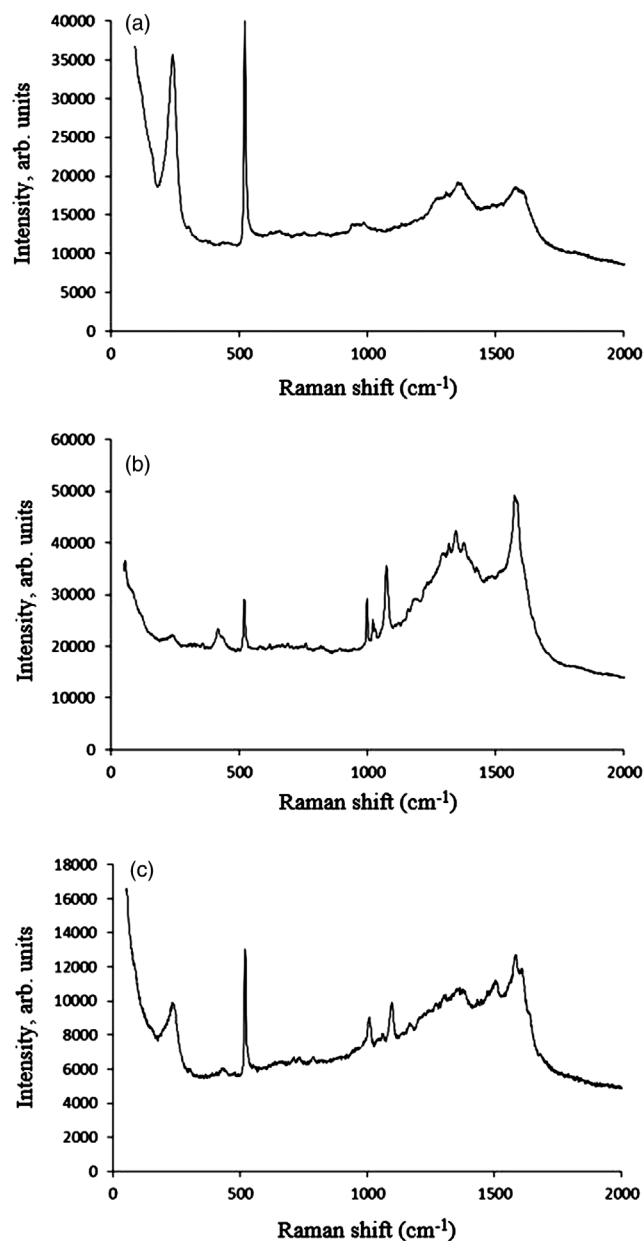


FIGURE 12 (a) Surface-enhanced Raman scattering (SERS) spectra of Suwannee River natural organic matter (SRNOM) coating on Au–Ag nanoparticles after 24 h. SERS spectra of Au–Ag nanoparticle coated with SRNOM for 24 h and afterwards exposed to (b) 4-mercaptobenzoic acid (4-MBA) or (c) mercaptopyridine (4-MPy) for 2 h

4 | CONCLUSIONS

Optimization parameters for SERS play a vital role in the reproducibility of the results, especially when the interaction of different coating agents at the same time is studied and each of the coating agents might require different SERS measurement parameters. These parameters can change the qualitative and especially quantitative results of the SERS measurements. After optimization of experimen-

tal parameters, competition of different coating agents was studied using the same setup. It was shown that 4-MPy has a higher binding affinity than SRNOM and 4-MBA through the presence of simultaneous S and N atoms. Therefore, 4-MPy dominates the coating process when two coating agents are present in the media at the same time. Furthermore, 4-MBA and 4-MPy bind to the SRNOM-coated NP despite the SRNOM coating already being formed.

Nanoparticles in the vadose zone experience changing environmental conditions. The detection of effects caused by changing environmental conditions on the coatings of NPs is very relevant to assess the environmental fate of NPs, whether they are released intentionally or unintentionally. Surface-enhanced-Raman scattering offers the possibility of directly detecting changes in NP coatings in natural environments.

CONFLICT OF INTEREST

The authors declare no conflict of interest.

ACKNOWLEDGMENTS

This research was funded by the Deutsche Forschungsgemeinschaft (DFG) within the research unit 1536 InterNano (Ba 1592/6-2). We thank Dr. George Metreveli (University Koblenz-Landau, Institute of Environmental Sciences) for ICP-MS and DLS characterization of NPs. We thank Dr. Carsten Peters (Technical University of Munich) for his assistance with TEM, and Christine Benning for conducting SEM measurements.

ORCID

Sayed Amininejad  <https://orcid.org/0000-0002-9365-4577>

Natalia P. Ivleva  <https://orcid.org/0000-0001-8762-119X>

Thomas Baumann  <https://orcid.org/0000-0002-0934-2715>

REFERENCES

- Aragay, G., Pino, F., & Merkoci, A. (2012). Nanomaterials for sensing and destroying pesticides. *Chemical Reviews*, *112*, 5317–5338. <https://doi.org/10.1021/cr300020c>
- Baalousha, M., Nur, Y., Römer, I., Tejamaya, M., & Lead, J. R. (2013). Effect of monovalent and divalent cations, anions and fulvic acid on aggregation of citrate-coated silver nanoparticles. *Science of the Total Environment*, *454*, 119–131. <https://doi.org/10.1016/j.scitotenv.2013.02.093>
- Bundschuh, M., Filser, J., Lüderwald, S., McKee, M. S., Metreveli, G., Schaumann, G. E., ... Wagner, S. (2018). Nanoparticles in the environment: Where do we come from, where do we go to? *Environmental Sciences Europe*, *30*. <https://doi.org/10.1186/s12302-018-0132-6>
- Cui, H., Li, S., Deng, S., Chen, H., & Wang, C. (2017). Flexible, transparent, and free-standing silicon nanowire SERS platform for in situ food inspection. *ACS Sensors*, *2*, 386–393. <https://doi.org/10.1021/acssensors.6b00712>

- Cui, L., Wu, D. Y., Wang, A., Ren, B., & Tian, Z. Q. (2010). Charge-transfer enhancement involved in the SERS of adenine on Rh and Pd demonstrated by ultraviolet to visible laser excitation. *The Journal of Physical Chemistry C*, *114*, 16588–16595. <https://doi.org/10.1021/jp1055717>
- Dai, S., Zhang, X., Du, Z., Huang, Y., & Dang, H. (2005). Structural properties and Raman spectroscopy of lipid Langmuir monolayers at the air–water interface. *Colloids and Surfaces B: Biointerfaces*, *42*, 21–28. <https://doi.org/10.1016/j.colsurfb.2004.12.021>
- Das, G., Mearini, F., Gentile, F., De Angelis, F., Kumar, H. M., Candeloro, P., ... Di Fabrizio, E. (2009). Nano-patterned SERS substrate: Application for protein analysis vs. temperature. *Biosensors and Bioelectronics*, *24*, 1693–1699. <https://doi.org/10.1016/j.bios.2008.08.050>
- Dreaden, E. C., Alkilany, A. M., Huang, X., Murphy, C. J., & El-Sayed, M. A. (2012). The golden age: Gold nanoparticles for biomedicine. *Chemical Society Reviews*, *41*, 2740–2779. <https://doi.org/10.1039/C1CS15237H>
- El Badawy, A. M., Aly Hassan, A., Scheckel, K. G., Suidan, M. T., & Tolaymat, T. M. (2013). Key factors controlling the transport of silver nanoparticles in porous media. *Environmental Science & Technology*, *47*, 4039–4045. <https://doi.org/10.1021/es304580r>
- El Badawy, A. M., Silva, R. G., Morris, B., Scheckel, K. G., Suidan, M. T., & Tolaymat, T. M. (2011). Surface charge-dependent toxicity of silver nanoparticles. *Environmental Science & Technology*, *45*, 283–287. <https://doi.org/10.1021/es1034188>
- Frimmel, F. H., & Niessner, R. (Eds.). (2014). *Nanoparticles in the water cycle*. Berlin, Heidelberg: Springer.
- Gao, J., Powers, K., Wang, Y., Zhou, H., Roberts, S. M., Moudgil, B. M., Koopman, B., & Barber, D. S. (2012). Influence of Suwannee River humic acid on particle properties and toxicity of silver nanoparticles. *Chemosphere*, *89*, 96–101. <https://doi.org/10.1016/j.chemosphere.2012.04.024>
- Guo, H., Zhang, Z., Xing, B., Mukherjee, A., Musante, C., White, J. C., & He, L. (2015). Analysis of silver nanoparticles in antimicrobial products using surface-enhanced Raman spectroscopy (SERS). *Environmental Science & Technology*, *49*, 4317–4324. <https://doi.org/10.1021/acs.est.5b00370>
- He, J., Wang, D., & Zhou, D. (2019). Transport and retention of silver nanoparticles in soil: Effects of input concentration, particle size and surface coating. *Science of the Total Environment*, *648*, 102–108. <https://doi.org/10.1016/j.scitotenv.2018.08.136>
- He, Y., Xiao, S., Dong, T., & Nie, P. (2019). Gold nanoparticles with different particle sizes for the quantitative determination of chlorpyrifos residues in soil by SERS. *International Journal of Molecular Sciences*, *20*(11). <https://doi.org/10.3390/ijms20112817>
- Ho, C.-H., & Lee, S. (2015). SERS and DFT investigation of the adsorption behavior of 4-mercaptobenzoic acid on silver colloids. *Colloids and Surfaces A: Physicochemical and Engineering Aspects*, *474*, 29–35. <https://doi.org/10.1016/j.colsurfa.2015.03.004>
- Huynh, K. A., & Chen, K. L. (2011). Aggregation kinetics of citrate and polyvinylpyrrolidone coated silver nanoparticles in monovalent and divalent electrolyte solutions. *Environmental Science & Technology*, *45*, 5564–5571. <https://doi.org/10.1021/es200157h>
- Kalachyova, Y., Lyutakov, O., Kostejn, M., Clupek, M., & Svorcik, V. (2015). Silver nanostructures: From individual dots to coupled strips for the tailoring of SERS excitation wavelength from near-UV to near-IR. *Electronic Materials Letters*, *11*, 288–294. <https://doi.org/10.1007/s13391-014-4336-7>
- Klitzke, S., Metreveli, G., Peters, A., Schaumann, G. E., & Lang, F. (2015). The fate of silver nanoparticles in soil solution: Sorption of solutes and aggregation. *Science of the Total Environment*, *535*, 54–60. <https://doi.org/10.1016/j.scitotenv.2014.10.108>
- Kneipp, K., Kneipp, H., Itzkan, I., Dasari, R. R., & Feld, M. S. (2002). Surface-enhanced Raman scattering and biophysics. *Journal of Physics: Condensed Matter*, *14*(18).
- Kühn, M., Ivleva, N. P., Klitzke, S., Niessner, R., & Baumann, T. (2015). Investigation of coatings of natural organic matter on silver nanoparticles under environmentally relevant conditions by surface-enhanced Raman scattering. *Science of The Total Environment*, *535*, 122–130. <https://doi.org/10.1016/j.scitotenv.2014.12.026>
- Kumari, G., Kandula, J., & Narayana, C. (2015). How far can we probe by SERS? *The Journal of Physical Chemistry C*, *119*, 20057–20064. <https://doi.org/10.1021/acs.jpcc.5b07556>
- Kurouski, D., & Van Duyne, R. P. (2015). In situ detection and identification of hair dyes using surface-enhanced Raman spectroscopy (SERS). *Analytical Chemistry*, *87*, 2901–2906. <https://doi.org/10.1021/ac504405u>
- Li, X., Lenhart, J. J., & Walker, H. W. (2010). Dissolution-accompanied aggregation kinetics of silver nanoparticles. *Langmuir*, *26*, 16690–16698. <https://doi.org/10.1021/la101768n>
- Lin, X., Lin, S., Liu, Y., Zhao, H., Liu, B., & Wang, L. (2019). Lab-on-paper surface-enhanced Raman spectroscopy platform based on self-assembled Au@Ag nanocube monolayer for on-site detection of thiram in soil. *Journal of Raman Spectroscopy*, *50*, 916–925. <https://doi.org/10.1002/jrs.5595>
- Marsich, L., Bonifacio, A., Mandal, S., Krol, S., Beleites, C., & Sergio, V. (2012). Poly-L-lysine-coated silver nanoparticles as positively charged substrates for surface-enhanced Raman scattering. *Langmuir*, *28*, 13166–13171. <https://doi.org/10.1021/la302383r>
- Moskovits, M. (2005). Surface-enhanced Raman spectroscopy: A brief retrospective. *Journal of Raman Spectroscopy*, *36*, 485–496. <https://doi.org/10.1002/jrs.1362>
- Philippe, A., & Schaumann, G. E. (2014). Interactions of dissolved organic matter with natural and engineered inorganic colloids: A review. *Environmental Science & Technology*, *48*, 8946–8962. <https://doi.org/10.1021/es502342r>
- Qian, X. M., & Nie, S. M. (2008). Single-molecule and single-nanoparticle SERS: From fundamental mechanisms to biomedical applications. *Chemical Society Reviews*, *37*, 912–920. <https://doi.org/10.1039/b708839f>
- Ren, B., Lin, X. F., Yang, Z. L., Liu, G. K., Aroca, R. F., Mao, B. W., & Tian, Z. Q. (2003). Surface-enhanced Raman scattering in the ultraviolet spectral region: UV-SERS on rhodium and ruthenium electrodes. *Journal of the American Chemical Society*, *125*, 9598–9599. <https://doi.org/10.1021/ja035541d>
- Rycenga, M., Cobley, C. M., Zeng, J., Li, W., Moran, C. H., Zhang, Q., ... Xia, Y. (2011). Controlling the synthesis and assembly of silver nanostructures for plasmonic applications. *Chemical Reviews*, *111*, 3669–3712. <https://doi.org/10.1021/cr100275d>
- Saha, S., Pal, A., Kundu, S., Basu, S., & Pal, T. (2009). Photochemical green synthesis of calcium-alginate-stabilized Ag and Au nanoparticles and their catalytic application to 4-nitrophenol reduction. *Langmuir*, *26*, 2885–2893. <https://doi.org/10.1021/la902950x>
- Schlücker, S. (2014). Surface-enhanced Raman spectroscopy: Concepts and chemical applications. *Angewandte Chemie International Edition*, *53*, 4756–4795. <https://doi.org/10.1002/anie.201205748>

- Shanthil, M., Thomas, R., Swathi, R. S., & George Thomas, K. (2012). Ag@SiO₂ core-shell nanostructures: Distance-dependent plasmon coupling and SERS investigation. *The Journal of Physical Chemistry Letters*, 3, 1459–1464. <https://doi.org/10.1021/jz3004014>
- Song, L., Mao, K., Zhou, X., & Hu, J. (2016). A novel biosensor based on Au@Ag core-shell nanoparticles for SERS detection of arsenic (III). *Talanta*, 146, 285–290. <https://doi.org/10.1016/j.talanta.2015.08.052>
- Stamplecoskie, K. G., Scaiano, J. C., Tiwari, V. S., & Anis, H. (2011). Optimal size of silver nanoparticles for surface-enhanced Raman spectroscopy. *The Journal of Physical Chemistry C*, 115, 1403–1409. <https://doi.org/10.1021/jp106666t>
- Stankus, D. P., Lohse, S. E., Hutchison, J. E., & Nason, J. A. (2011). Interactions between natural organic matter and gold nanoparticles stabilized with different organic capping agents. *Environmental Science & Technology*, 45, 3238–3244. <https://doi.org/10.1021/es102603p>
- Sun, T. Y., Gottschalk, F., Hungerbühler, K., & Nowack, B. (2014). Comprehensive probabilistic modelling of environmental emissions of engineered nanomaterials. *Environmental Pollution*, 185, 69–76. <https://doi.org/10.1016/j.envpol.2013.10.004>
- Tian, F., Bonnier, F., Casey, A., Shanahan, A. E., & Byrne, H. J. (2014). Surface enhanced Raman scattering with gold nanoparticles: Effect of particle shape. *Analytical Methods*, 6, 9116–9123. <https://doi.org/10.1039/C4AY02112F>
- Valley, N., Greeneltch, N., Van Duyne, R. P., & Schatz, G. C. (2013). A look at the origin and magnitude of the chemical contribution to the enhancement mechanism of surface-enhanced Raman spectroscopy (SERS): Theory and experiment. *The Journal of Physical Chemistry Letters*, 4, 2599–2604. <https://doi.org/10.1021/jz4012383>
- Wang, Z., & Rothberg, L. J. (2005). Origins of blinking in single-molecule Raman spectroscopy. *The Journal of Physical Chemistry B*, 109, 3387–3391. <https://doi.org/10.1021/jp0460947>
- Wang, Z., Zhang, L., Zhao, J., & Xing, B. (2016). Environmental processes and toxicity of metallic nanoparticles in aquatic systems as affected by natural organic matter. *Environmental Science: Nano*, 3, 240–255. <https://doi.org/10.1039/C5EN00230C>
- Wei, H., Abtahi, S. M. H., & Vikesland, P. J. (2015). Plasmonic colorimetric and SERS sensors for environmental analysis. *Environmental Science: Nano*, 2, 120–135. <https://doi.org/10.1039/C4EN00211C>
- Wen, Z. (2007). Raman spectroscopy of protein pharmaceuticals. *Journal of Pharmaceutical Sciences*, 96, 2861–2878. <https://doi.org/10.1002/jps.20895>
- Xu, M. L., Gao, Y., Han, X. X., & Zhao, B. (2017). Detection of pesticide residues in food using surface-enhanced Raman spectroscopy: A review. *Journal of Agricultural and Food Chemistry*, 65, 6719–6726. <https://doi.org/10.1021/acs.jafc.7b02504>
- Yaffe, N. R., Ingram, A., Graham, D., & Blanch, E. W. (2009). A multi-component optimisation of experimental parameters for maximising SERS enhancements. *Journal of Raman Spectroscopy*, 41, 618–623. <https://doi.org/10.1002/jrs.2495>
- Yuan, H., Fales, A. M., Khoury, C. G., Liu, J., & Vo-Dinh, T. (2013). Spectral characterization and intracellular detection of surface-enhanced Raman scattering (SERS)-encoded plasmonic gold nanostars: Nanostars SERS characterization. *Journal of Raman Spectroscopy*, 44, 234–239. <https://doi.org/10.1002/jrs.4172>
- Zhang, L., Bai, Y., Shang, Z., Zhang, Y., & Mo, Y. (2007). Experimental and theoretical studies of Raman spectroscopy on 4-mercaptopyridine aqueous solution and 4-mercaptopyridine/Ag complex system. *Journal of Raman Spectroscopy*, 38, 1106–1111. <https://doi.org/10.1002/jrs.1719>
- Zhao, J., Zhang, K., Li, Y., Ji, J., & Liu, B. (2016). High-resolution and universal visualization of latent fingerprints based on aptamer-functionalized core-shell nanoparticles with embedded SERS reporters. *ACS Applied Materials & Interfaces*, 8, 14389–14395. <https://doi.org/10.1021/acsami.6b03352>
- Zheng, X. S., Hu, P., Zhong, J. H., Zong, C., Wang, X., Liu, B. J., & Ren, B. (2014). Laser power dependent surface-enhanced Raman spectroscopic study of 4-mercaptopyridine on uniform gold nanoparticle-assembled substrates. *The Journal of Physical Chemistry C*, 118, 3750–3757. <https://doi.org/10.1021/jp409711r>

How to cite this article: Amininejad S, Ivleva NP, Baumann T. Characterization of coatings on metallic nanoparticles by surface-enhanced Raman scattering (SERS) for environmental purposes. *Vadose Zone J.* 2020;19:e20076. <https://doi.org/10.1002/vzj2.20076>